

Article

First Principle Study of MgSnLa Compounds in Mg-3Sn-1Mn-1La Alloy Processed by Rheo-Rolling

Jian-Hong Wang  and Zhan-Yong Zhao *

School of Materials Science and Engineering, North University of China, Taiyuan 030051, China;
wangjianhong@nuc.edu.cn

* Correspondence: zhaozy@nuc.edu.cn

Abstract: In order to obtain a high-performance heat-resistant Mg alloy during the rheo-rolling process, the electronic structure, elastic constants, binding energy and thermodynamic properties of the MgSnLa compounds were conducted by first-principle calculations. The results show that the MgSnLa compounds (La_5Sn_3 , $\text{Mg}_{17}\text{La}_2$ and Mg_2Sn) all show certain metallicity, and La_5Sn_3 has better mechanical properties (higher bulk modulus (46.47091 GPa) and shear modulus (26.40561 GPa)) than the other two phases. The binding energy reveals that La_5Sn_3 is the most stable phase in these composite phases (5.33 eV/atom); additionally, thermodynamic studies show that the structural stability of the MgSnLa compounds increases with the increase in temperature, and the temperature has the greatest effect on the stability of $\text{Mg}_{17}\text{La}_2$. These all provide an efficient guide for the widespread engineering applications of high-performance heat-resistant Mg alloy.

Keywords: heat-resistant Mg alloy; rheo-rolling; first principle; thermodynamic properties; MgSnLa compounds



Citation: Wang, J.-H.; Zhao, Z.-Y. First Principle Study of MgSnLa Compounds in Mg-3Sn-1Mn-1La Alloy Processed by Rheo-Rolling. *Materials* **2022**, *15*, 1361. <https://doi.org/10.3390/ma15041361>

Academic Editor: Elena Villa

Received: 16 December 2021

Accepted: 10 February 2022

Published: 12 February 2022

Publisher's Note: MDPI stays neutral with regard to jurisdictional claims in published maps and institutional affiliations.



Copyright: © 2022 by the authors. Licensee MDPI, Basel, Switzerland. This article is an open access article distributed under the terms and conditions of the Creative Commons Attribution (CC BY) license (<https://creativecommons.org/licenses/by/4.0/>).

1. Introduction

Magnesium (Mg) alloys are widely used in automotive, aerospace and other fields because of their low density, excellent mechanical properties, strong anti-electromagnetic interference and excellent electromagnetic shielding ability. The main way to improve the strength and heat resistance of magnesium alloys is micro-alloying. On the one hand, microalloying could form a strengthening phase on the grain boundary, pinning the grain boundary to inhibit grain boundary slip; on the other hand, it could also play the effect of solid solution strengthening and precipitation strengthening in the matrix. Hence, the thermal stability of the strengthening phase is critical to the mechanical properties of Mg alloys.

In recent decades, introducing Sn element into Mg alloys has been proposed to form the Mg_2Sn strengthening phase with high-temperature resistance. Additionally, its melting point (778 °C) is much higher than that of the $\text{Mg}_{17}\text{Al}_{12}$ phase (498 °C) in traditional AZ Mg alloys, and the hardness value is up to 119 HV [1,2]. Therefore, it could be concluded that the Mg_2Sn phase is an excellent heat-resistant Mg alloy strengthening phase [3]. Radha et al. [4] researched the microstructure, mechanical and corrosion properties of as-cast Mg-1wt%Sn-5wt% HA (hydroxyapatite) composites, and pointed out that the introduction of Sn could effectively refine the grain size and form Mg_2Sn strengthening phase along the grain boundary, which improved the mechanical and corrosion properties of the composite alloy. Zhao et al. [5] reported the effect of Sn content on strain hardening behavior of as-extruded Mg-xSn ($x = 1.3, 2.4, 3.6$ and 4.7 wt%) binary alloy, and pointed out that the as-extruded Mg-Sn alloys mainly included α -Mg matrix and second phase Mg_2Sn . Moreover, they concluded a view that Sn content weakened the strain hardening ability of as-extruded Mg-Sn alloys, but yielded an obvious elevation in its tensile strength, yield strength and elongation.

To improve the high-temperature mechanical properties of Mg-Sn alloy, some researchers added rare earth (RE) and other elements into the Mg alloy. Wei et al. [6] revealed that the feather-shaped, rod-like and massive rare earth phases formed in Mg-Sn-La alloys are the main internal factors for its better properties than as-cast Mg-5Sn alloy. Liu et al. [7] studied the microstructure and mechanical properties of permanent-mold cast Mg-5 wt% Sn-(0-2.6) wt% Di alloys (neodymium: praseodymium = 3:1), and found that the formation of $\text{Sn}_x(\text{Nd, Pr})_y$ phase is promoted by the electronegativity difference between different elements. Moreover, they revealed that the strong segregation effect and the Sn-Di phase formed in the melt, hinder the rapid growth of crystals that would refine the grains. All these help to improve the creep resistance of the composite alloy. Pan et al. [8] investigated and compared the microstructure evolution and mechanical properties via adding Zr, Se and Ce on the as-cast Mg-3Sn-1Mn (wt.%) alloy, and concluded that adding 0.36 wt.% SC and 0.87 wt.% Ce could lead to the formation of extra phases of Mg-Sn-Sc and Mg_{12}Ce , also adding 0.43 wt.% Zr or 0.87 wt.% Ce could refine the grains, these results all played a positive role in improving the tensile or creep properties of the alloy. Wang et al. [9] addressed the microstructure, tensile properties and compressive creep behaviors of the Mg-(1.65-11.52) wt.% Sn-2 wt.% Nd alloys, and dendritic α -Mg, Mg_2Sn and Mg-Sn-Nd ternary phase could be observed. In addition, when a composition of Mg-8.23 wt.% Sn-2 wt.% Nd is determined, the highest ultimate tensile strength could be up to 140 MPa.

In the heat-resistant magnesium alloy system, Mg-Sn alloy can form Mg_2Sn strengthening phase with high-temperature resistance and high hardness; Particularly, to further improve the high-temperature mechanical properties of Mg-Sn alloys, the researchers further found that Mn and rare earth (RE) element La play an important role in improving the mechanical properties and corrosion properties of Mg Sn alloys due to solid solution strengthening, fine grain strengthening and the formation of MgSnLa compounds [10,11]. However, considering that the structure and properties of the MgSnLa compounds are still unclear. Here, we report its structure properties through the first principle, providing an efficient guide for the widespread engineering applications of high-performance heat-resistant Mg alloy.

2. Computational and Experimental Procedure

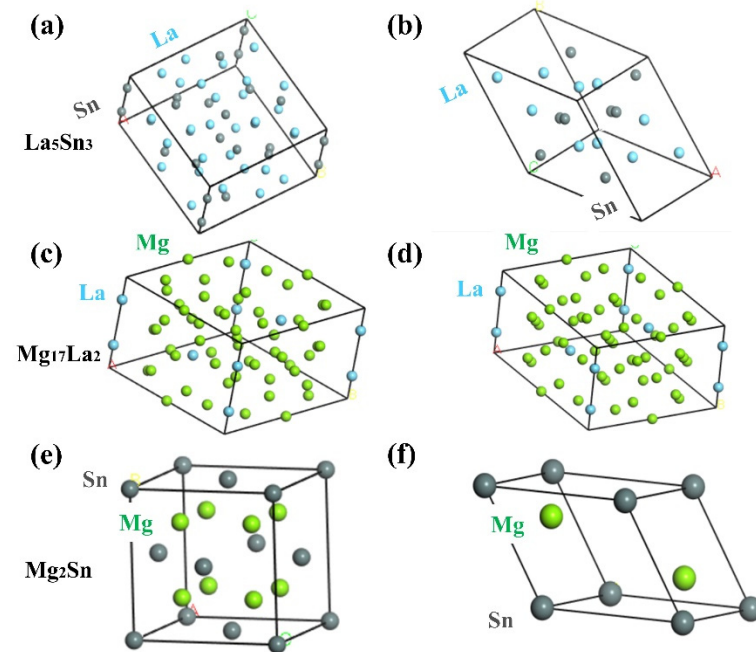
First principle calculations were performed using Cambridge Serial Total Energy Package (CASTEP) module in Materials Studio 8.0 (Accelrys, Inc. an Diego, CA, USA), which is based on the density-functional theory (DFT). It should be noted that the appropriate plane-wave energy cutoff, Monkhorst-Pack k-point grid were considered before the calculation, so as to ensure the accuracy of the calculation. Table 1 shows the crystal structure parameters of La_5Sn_3 , $\text{Mg}_{17}\text{La}_2$ and Mg_2Sn [2,12,13]. The Broyden Fletcher Goldfarb Shannon (BFGS) algorithm was used to achieve the geometric optimization of the structural model in this paper (Table 2 and Figure 1), which can accurately minimize the total energy of the system in an iterative way. Moreover, the convergence criteria containing maximum stress, maximum force and maximum displacements were set within a reasonable range.

Table 1. Crystal structure parameters of La_5Sn_3 , $\text{Mg}_{17}\text{La}_2$ and Mg_2Sn .

Phases	La_5Sn_3	$\text{Mg}_{17}\text{La}_2$	Mg_2Sn
Space group	14/MCM (140)	P63/MMC (194)	FM-3M (225)
Lattice constants	$a = b = 12.749 \text{ \AA}$, $c = 6.343 \text{ \AA}$	$a = b = 10.35 \text{ \AA}$, $c = 10.28 \text{ \AA}$	$a = b = c = 6.81 \text{ \AA}$
Atomic coordinates	La (0, 0.5, 0.25), Sn (0, 0, 0.25)	La (0, 0, 0.25), Mg (0.333, 0.666, 0.11)	Mg (0.25, 0.25, 0.25), Sn (0, 0, 0)

Table 2. Lattice constants of La_5Sn_3 , Mg_2Sn and $\text{Mg}_{17}\text{La}_2$ before and after geometric optimization.

Phases	Optimal State	a (Å)	b (Å)	c (Å)	α	β	γ
La_5Sn_3	before optimization	12.749	12.749	6.343	90°	90°	90°
	after optimization	9.687	9.687	9.687	96.31°	96.31°	141.3°
$\text{Mg}_{17}\text{La}_2$	before optimization	10.35	10.35	10.28	90°	90°	120°
	after optimization	10.43	10.43	10.16	90°	90°	120°
Mg_2Sn	before optimization	6.81	6.81	6.81	90°	90°	90°
	after optimization	4.83	4.83	4.83	60°	60°	60°

**Figure 1.** Cell models of La_5Sn_3 , $\text{Mg}_{17}\text{La}_2$ and Mg_2Sn before and after geometric optimization: (a,c,e) before geometric optimization and (b,d,f) after geometric optimization.

Mg - 3Sn - 1Mn alloy is prepared by melting magnesium ingot (magnesium content > 99.9%), tin ingot (aluminum content > 99.9%) and manganese agent (manganese content: 80%); in particular, La element is added in the form of Mg-La master alloy. Mg- 3Sn - 1Mn -La alloys (15 mm \times 15 mm \times 10 mm) was prepared by continuous rheological rolling, and a detailed description of Mg- 3Sn - 1Mn - 1La alloy could be found in our previous reports [11,14,15]. The specific advantages of the rheo-rolling process are as follows: (1) The vibration method effectively prevents the slurry from sticking on the surface of the inclined plate, which is efficient and convenient; (2) compared with roll casting, there is no need for complex side seal control; (3) the rolling speed is high, which is higher than the full liquid casting rolling speed.

Transmission electron microscope (TEM) characterization was performed by field-emission-gun (FEG) Tecnai G² 20 microscope (FEI, Hillsboro, OR, USA) equipped with energy dispersive spectroscopy (EDS). The identification of the precipitates in the Mg- 3Sn - 1Mn - 1La alloys was performed in an X-ray diffraction (XRD) (X'Pert, PANalytical B.V., Almelo, Holland).

3. Results and Discussion

Figure 2 displays a complete high angle annular dark field-scanning transmission electron microscopy (HAADF-STEM) image of the Mg- 3Sn - 1Mn - 1La alloy where the dark area (plate-like compounds) mainly contains Mg, Sn and La elements, and XRD further proved that the plate-like compounds were composed of La_5Sn_3 , Mg_2Sn and $\text{Mg}_{17}\text{La}_2$ phases (Figure 3). Among them, the identification of the Mg_2Sn phase was confirmed by

the high-resolution transmission electron microscopy (HRTEM) and the Fourier transform (FT) pattern (Figure 4). The HRTEM of other phases (La_5Sn_3 and $\text{Mg}_{17}\text{La}_2$) have been reported in our previous studies [14].

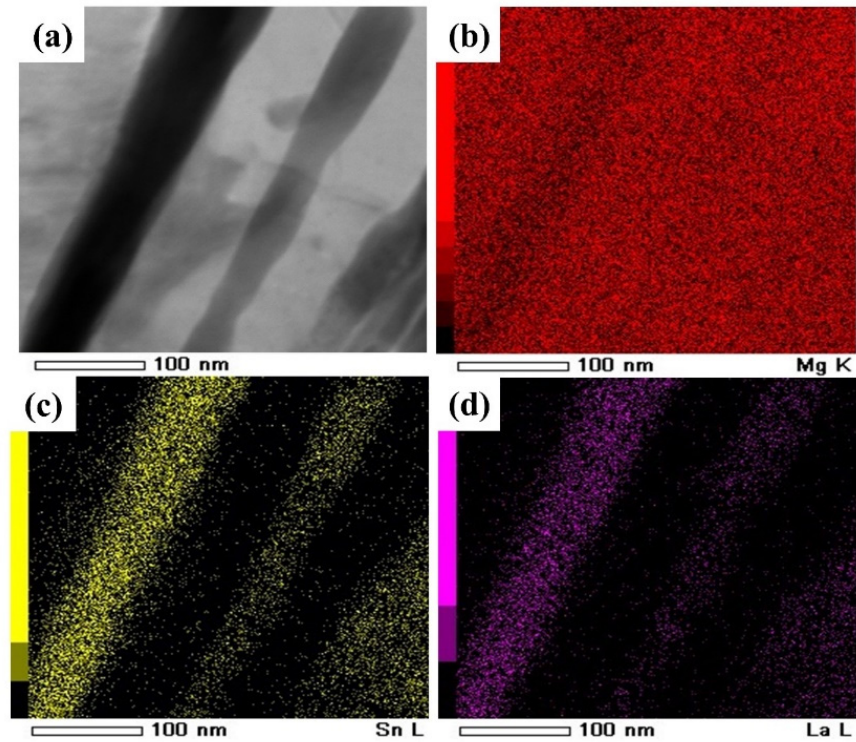


Figure 2. (a) HADDF-STEM image of Mg-3Sn-1Mn-1La alloy, (b–d) EDS map of Mg, Sn and La elements, respectively.

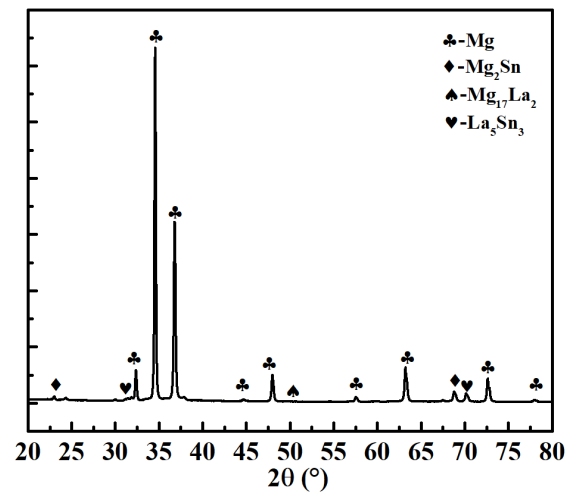


Figure 3. XRD pattern of the Mg-3Sn-1Mn-1La alloys showing the Mg, La_5Sn_3 , Mg_2Sn and $\text{Mg}_{17}\text{La}_2$ phases.

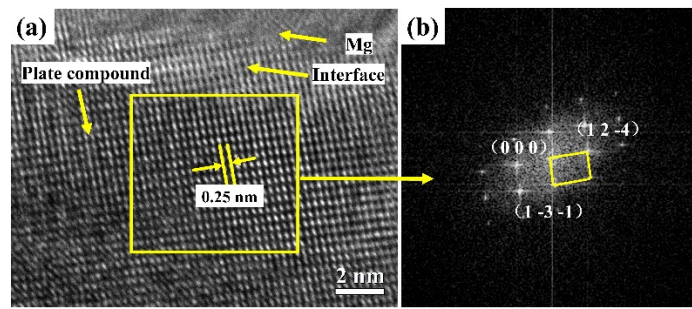


Figure 4. (a) HRTEM image of Mg-3Sn-1Mn-1La alloy, (b) FT map of the selective yellow box in (a).

In the present work, the energy band structures and density of states (DOS) are calculated to have a profound insight into the bonding of La_5Sn_3 , $\text{Mg}_{17}\text{La}_2$ and Mg_2Sn phases [16]. In Figure 5, the Fermi levels of the three phases intersect the conduction band (Figure 5a,c,e), and the partial density of states (PDOS) of La and Mg cross the Fermi level E_f (Figure 5b,d,f), indicating that the three phases have metal properties.

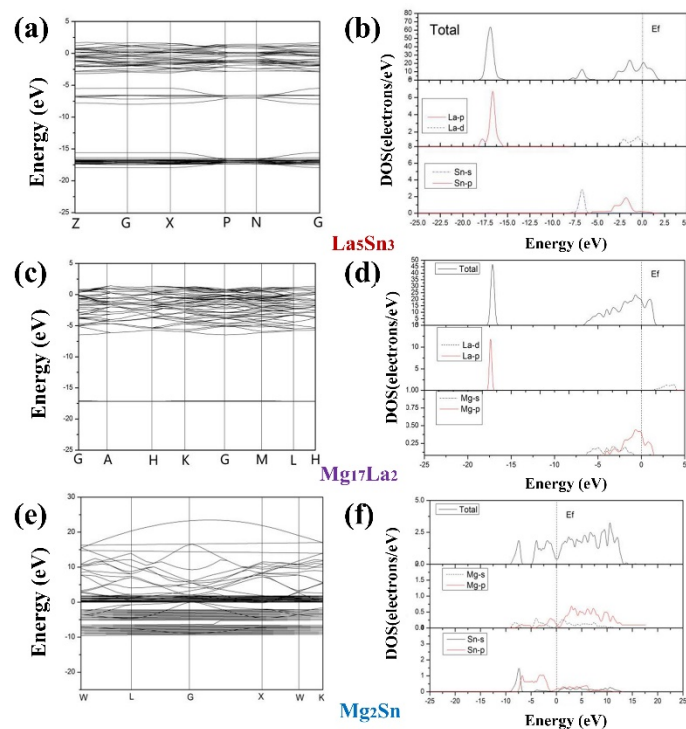


Figure 5. Detailed energy-band structures and density of states of La_5Sn_3 , $\text{Mg}_{17}\text{La}_2$ and Mg_2Sn : (a,c,e) band structures and (b,d,f) density of states.

Further, it could be seen that the total DOS of the La_5Sn_3 phase (Figure 5b) could be divided into three regions: one region ranges from -18 to 15 eV, and the DOS of this region is mainly contributed to by the $5p$ state of La; the other is at -7.5 – 6 eV, this DOS of the region is mainly contributed to by the $5s$ state of Sn; while the DOS at the conduction band is mainly contributed to by the $5d$ state of La and a small amount of $5p$ states of Sn. All these indicate that the strong hybridization of La $5d$ and Sn $5p$ orbitals makes a great contribution to the metal properties of La_5Sn_3 . For $\text{Mg}_{17}\text{La}_2$, the total DOS is roughly divided into two regions: one region is located at 16 eV– 18 eV, and the DOS in this region is contributed to by the $5d$ state of La; the other conduction band region is mainly contributed by the $2p$ and $3s$ orbits of Mg; moreover, it can be seen from the energy band diagram (Figure 5c) that the $5d$ orbital of La is a straight line, indicating that La does not participate in hybridization. However, as for the Mg_2Sn (Figure 5e), the wide energy band and the

great fluctuation of the energy band promote the strong expansibility of the atomic orbitals that make up the energy band. Meanwhile, from Figure 5f, it can be concluded that the energy band is hybrid from the s and p orbitals of Mg and the s and p orbitals of Sn.

Elastic constants play a great role in characterizing the elastic properties of materials, and occupy an important position in the mechanical properties of materials. Moreover, the calculation of crystal elastic constants is closely related to the symmetry of crystal cells, and the calculated independent elastic constants are different under different crystal systems. Hence, this paper only discussed the independent elastic constants of tetragonal, hexagonal and cubic crystal structures.

For the tetragonal crystal structure, there are six independent elastic constants: C_{11} , C_{12} , C_{13} , C_{33} , C_{44} and C_{66} . The elastic stability criterion of the tetragonal crystal structure is:

$$C_{11} > 0, C_{33} > 0, C_{44} > 0, C_{11} - C_{12} > 0, 2(C_{11} + C_{12}) + C_{33} + 4C_{13} > 0 \quad (1)$$

$$C_{66} > 0, C_{11} + C_{33} - 2C_{13} > 0 \quad (2)$$

For hexagonal crystal structure, there are five independent elastic constants: C_{11} , C_{12} , C_{13} , C_{33} and C_{44} . The elastic stability criterion of the hexagonal crystal structure is:

$$C_{11} > |C_{12}|, (C_{11} + 2C_{12}) C_{33} > 2 C_{13}^2 \quad (3)$$

For cubic crystal structure, there are three independent elastic constants: C_{11} , C_{12} and C_{44} . The elastic stability criterion of this cubic crystal structure is:

$$C_{11} > 0, C_{44} > 0, C_{11} - C_{12} > 0, C_{11} + 2C_{12} > 0 \quad (4)$$

In summary, La_5Sn_3 with tetragonal crystal structure, $\text{Mg}_{17}\text{La}_2$ with hexagonal crystal structure, and Mg_2Sn with cubic crystal structure have been verified to meet their corresponding stability criteria (Table 3). Furthermore, it is found from Figure 6 that the La_5Sn_3 phase has higher bulk modulus and shear modulus values than the other two phases, indicating that the La_5Sn_3 phase has higher mechanical properties.

Table 3. Elastic constants of C_{ij} (GPa).

Phases	C11	C12	C13	C33	C44	C66
La_5Sn_3	92.47	33.56	25.13	70.99	22.09	32.36
$\text{Mg}_{17}\text{La}_2$	69.98	21.21	19.12	80.78	22.73	-
Mg_2Sn	58.45	29.65	-	-	27.91	-

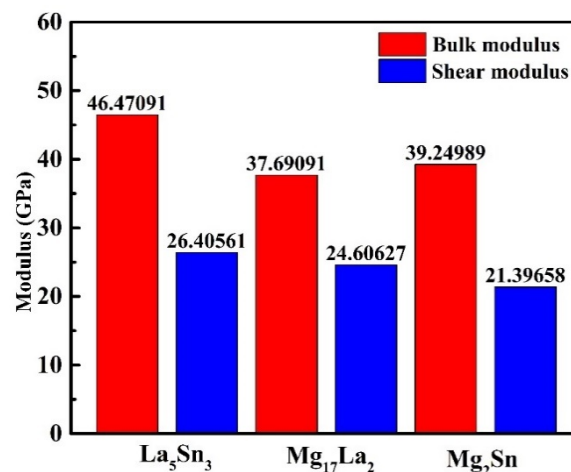


Figure 6. The bulk modulus and shear modulus values of La_5Sn_3 , $\text{Mg}_{17}\text{La}_2$ and Mg_2Sn .

Binding energy is one of the conditions describing the stability of phase structure. It represents the energy required to split a cell structure into a single atom or the energy released when a single atom is combined into a cell. The calculation method is as follows [17]:

$$E_{coh} = \frac{1}{x+y} (E_{tot} - xE_{atom}^A - yE_{atom}^B) \quad (5)$$

In the formula, E_{tot} is the total energy of the cell, E_{atom}^A , E_{atom}^B represents the energy of A and B free atoms, and x and y represent the number of atoms of A and B atoms in the cell structure model, respectively. The same conditions as the total energy of the intermetallic compound cell are used in calculating the free atom energy.

On the one hand, the forming ability of the alloy can be calculated and compared by the enthalpy of alloy formation. The calculation formula is as follows:

$$\Delta H = \frac{E_{tot}^{AB} - N_A E_{solid}^A - N_B E_{solid}^B}{N_A + N_B} \quad (6)$$

where ΔH is the enthalpy of alloy formation; E_{tot}^{AB} is the total energy of intermetallic compounds; E_{solid}^A and E_{solid}^B represent the (average energy)/(each atom) of A and B in the solid-state; N_A and N_B are the number of atoms A and B in the cell.

It can be seen from Table 4 that the enthalpy of formation of La_5Sn_3 , $\text{Mg}_{17}\text{La}_2$ and Mg_2Sn is negative, indicating that these phases can be formed, and the process is an exothermic reaction. Moreover, the larger the absolute value of the enthalpy of formation, the stronger the phase formation ability [18,19]. Therefore, it can be concluded that Mg_2Sn has the strongest formation ability, followed by La_5Sn_3 , and $\text{Mg}_{17}\text{La}_2$ is the worst. For the binding energy, it refers to the energy released by combining free atoms into crystals; the larger the value of energy, the more stable the formed crystals; therefore, it can be seen that La_5Sn_3 is the most stable, followed by $\text{Mg}_{17}\text{La}_2$ and finally Mg_2Sn .

Table 4. The binding energy and enthalpy of formation of La_5Sn_3 , $\text{Mg}_{17}\text{La}_2$ and Mg_2Sn .

Phases	E/(eV/Atom)	H/(eV/Atom)
La_5Sn_3	5.33	−1.03
$\text{Mg}_{17}\text{La}_2$	2.48	−0.65
Mg_2Sn	0.17	−6.3

On the other hand, the calculation of the thermodynamic performance of the system follows the standard thermodynamic statistical formula. The enthalpy (H) of the system and the Gibbs free energy (G) at each temperature are calculated by the following formula:

$$H = U + \int c_p dT \quad (7)$$

$$G = H - TS \quad (8)$$

where: T is the temperature; c_p is the constant pressure-specific heat capacity at this temperature; U is the heat of formation at 0 K, 1.01×10^5 Pa, and S is the entropy at the corresponding temperature.

The quasi-harmonic Debye model is used to calculate the changes of enthalpy, entropy and Gibbs free energy of each phase with temperature [20]. When the temperature increases from 298 K (room temperature) to 1000 K, the entropy and enthalpy of the MgSnLa compounds (La_5Sn_3 , $\text{Mg}_{17}\text{La}_2$ and Mg_2Sn) increase (Figure 7a,b). On the contrary, Gibbs free energy decreases with the temperature increasing (Figure 7c), indicating that the structural stability of the MgSnLa compounds increases with the increase in temperature. Further analysis found that as the temperature increases, the free energy of $\text{Mg}_{17}\text{La}_2$ is most sensitive to temperature changes, and the downward trend is the largest, followed by La_5Sn_3 , and Mg_2Sn is the least sensitive. This may be related to the poor alloying ability of $\text{Mg}_{17}\text{La}_2$.

This reveals that with the introduction of La, the structural stability of the Mg alloy system changes slightly with the increase in temperature; that is, the structural stability of $Mg_{17}La_2$ changes from less stable than Mg_2Sn and La_5Sn_3 to more stable than them. Hence, it can be concluded that improving the thermodynamic stability of the alloy can be considered by increasing the temperature of the alloy. Moreover, the order of thermal stability of the three structures does not change significantly with the increase in temperature from 350 K to 675 K (Figure 7c).

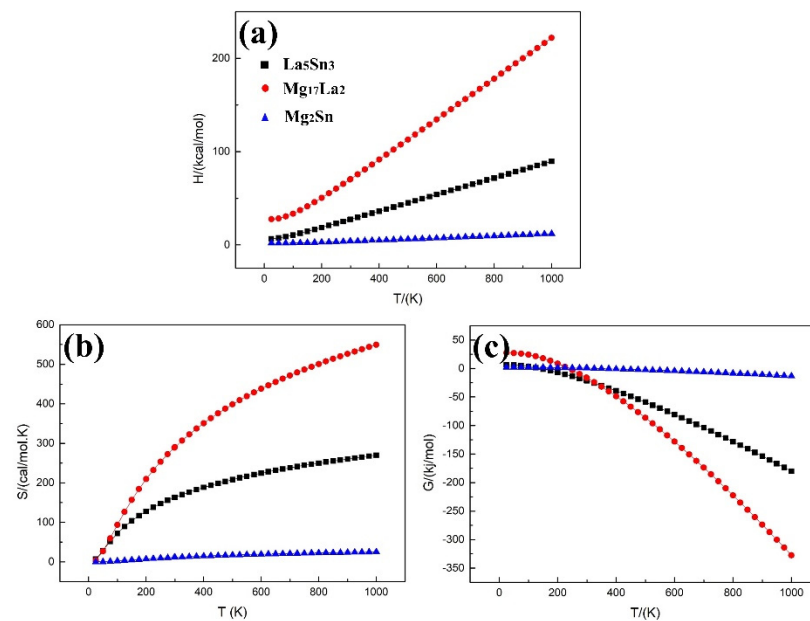


Figure 7. The enthalpy, entropy, and Gibbs free energy change of La_5Sn_3 , $Mg_{17}La_2$, and Mg_2Sn at different temperatures: (a) the enthalpy change, (b) the entropy change, and (c) Gibbs free energy change.

4. Conclusions

In this study, the performance of MgSnLa compounds was compared by the first principle calculations, and the main conclusions are as follows:

- (1) According to the calculation results, MgSnLa compounds (La_5Sn_3 , $Mg_{17}La_2$ and Mg_2Sn) all show certain metallicity, and La_5Sn_3 has better mechanical properties (higher bulk modulus and shear modulus) than the other two phases.
- (2) For the binding energy, it can be concluded that La_5Sn_3 is the most stable, followed by $Mg_{17}La_2$ and finally Mg_2Sn .
- (3) The structural stability of the MgSnLa compounds increases with the increase in temperature.
- (4) As the temperature increases, the free energy of $Mg_{17}La_2$ is most sensitive to temperature changes, and the downward trend is the largest, followed by La_5Sn_3 , and Mg_2Sn is the least sensitive.

Author Contributions: J.-H.W. designed the research plan, wrote and revised the paper. Z.-Y.Z. is responsible for reviewing and editing the article. All authors have read and agreed to the published version of the manuscript.

Funding: This research was funded by Major Science and Technology Projects of Shanxi Province, China (Grant No.20181101009).

Institutional Review Board Statement: Not applicable.

Informed Consent Statement: Not applicable.

Data Availability Statement: All the data is available within the manuscript.

Conflicts of Interest: The authors declare no conflict of interest.

References

1. Chen, Y.; Jin, L.; Li, W.; Song, Y.; Hao, L. Microstructure and mechanical properties of as aged Mg–3Sn–1Al and Mg–3Sn–2Zn–1Al alloy. *Mater. Sci. Technol.* **2015**, *31*, 73–78. [[CrossRef](#)]
2. Li, Y.; Zhao, Y.H.; Yang, X.M.; Hou, H. Mechanical and Thermodynamic Properties of Mg₁₇La₂, La₅Si₄ and La₅Sn₃ Phases in Mg–Sn–Mn (Si)–La Alloy from First-Principles Calculations. *Sci. Adv. Mater.* **2020**, *12*, 1649–1655.
3. Luo, J.; Chen, R.S.; Han, E.H. Effects of Gd on the Microstructure and Mechanical Properties of Mg–3Sn Alloys. *Mater. Sci. Forum* **2013**, *747–748*, 245–250. [[CrossRef](#)]
4. Radha, R.; Sreekanth, D. Mechanical and corrosion behaviour of hydroxyapatite reinforced Mg–Sn alloy composite by squeeze casting for biomedical applications. *J. Magnes. Alloy* **2020**, *8*, 452–460. [[CrossRef](#)]
5. Zhao, C.Y.; Chen, X.H.; Pan, F.S.; Gao, S.Y.; Zhao, D.; Liu, X.F. Effect of Sn content on strain hardening behavior of as-extruded Mg–Sn alloys. *Mater. Sci. Eng. A* **2018**, *713*, 244–252. [[CrossRef](#)]
6. Wei, S.H.; Chen, Y.G.; Tang, Y.B.; Zhang, X.P.; Liu, M.; Xiao, S.F.; Zhao, Y.H. Compressive creep behavior of Mg–Sn–La alloys. *Mater. Sci. Eng. A* **2009**, *508*, 59–63. [[CrossRef](#)]
7. Liu, H.M.; Chen, Y.G.; Tang, Y.B.; Huang, D.M.; Niu, G. The microstructure and mechanical properties of permanent-mould cast Mg–5wt%Sn–(0–2.6)wt%Di alloys. *Mater. Sci. Eng. A* **2006**, *437*, 348–355. [[CrossRef](#)]
8. Pan, F.S.; Yang, M.B. Preliminary investigations about effects of Zr, Sc and Ce additions on as-cast microstructure and mechanical properties of Mg–3Sn–1Mn (wt.%) magnesium alloy. *Mater. Sci. Eng. A* **2011**, *528*, 4973–4981. [[CrossRef](#)]
9. Wang, Q.; Chen, Y.G.; Xiao, S.F.; Zhang, X.P.; Tang, Y.B.; Wei, S.H.; Zhao, Y.H. Study on microstructure and mechanical properties of as-cast Mg–Sn–Nd alloys. *J. Rare Earths* **2010**, *28*, 790–793. [[CrossRef](#)]
10. Zhao, Z.Y.; Guan, R.G.; Shen, Y.F.; Bai, P.K. Grain refinement mechanism of Mg–3Sn–1Mn–1La alloy during accumulative hot rolling. *J. Mater. Sci. Technol.* **2021**, *91*, 251–261. [[CrossRef](#)]
11. Zhao, Z.Y.; Bai, P.K.; Guan, R.G.; Murugadoss, V.; Liu, H.; Wang, X.J.; Guo, Z.H. Microstructural evolution and mechanical strengthening mechanism of Mg–3Sn–1Mn–1La alloy after heat treatments. *Mater. Sci. Eng. A* **2018**, *734*, 200–209. [[CrossRef](#)]
12. Evdokimenko, V.I.; Kripyakevich, P.I. Über die Löslichkeit von Lanthan in Aluminium, Magnesium und den homogenen Legierungen des Magnesiums und Aluminiums. *Z. Electrochem. Angew. Phys. Chem.* **1940**, *46*, 357–364.
13. Franceschi, E.A. Dimorphism of La₅Sn₃, Ce₅Sn₃ and Pr₅Sn₃ compounds. *J. Less Common Met.* **1979**, *66*, 175–181. [[CrossRef](#)]
14. Guan, R.G.; Shen, Y.F.; Zhao, Z.Y.; Misra, R.D.K. Nanoscale precipitates strengthened lanthanum-bearing Mg–3Sn–1Mn alloys through continuous rheo-rolling. *Sci. Rep.* **2016**, *6*, 23154. [[CrossRef](#)] [[PubMed](#)]
15. Guan, R.G.; Zhao, Z.Y.; Zhang, H.; Lian, C.; Lee, C.S.; Liu, C.M. Microstructure evolution and properties of Mg–3Sn–1Mn (wt%) alloy strip processed by semisolid rheo-rolling. *J. Mater. Process. Technol.* **2012**, *212*, 1430–1436. [[CrossRef](#)]
16. Zheng, B.; Zhao, L.; Hu, X.B.; Dong, S.J.; Li, H. First-principles studies of Mg₁₇Al₁₂, Mg₂Al₃, Mg₂Sn, MgZn₂, Mg₂Ni and Al₃Ni phases. *Phys. B* **2019**, *560*, 255–260. [[CrossRef](#)]
17. Wu, H.Y.; Dong, Y.P.; Li, X.W.; Li, Y.L.; Yan, M. First principle calculations and low cost SLM processing of Ti–TiB composite materials. *Mater. Sci. Eng. A* **2021**, *803*, 140711. [[CrossRef](#)]
18. Martin, A.C.; Oliveira, J.P.; Fink, C. Elemental effects on weld cracking susceptibility in Al_xCoCrCuFeNi high-entropy alloy. *Metall. Mater. Trans. A* **2020**, *51*, 778–787. [[CrossRef](#)]
19. Oliveira, J.P.; Shen, J.; Zeng, Z.; Park, J.M.; Choi, Y.T.; Schell, N.; Maawad, E.; Zhou, N.; Kim, H.S. Dissimilar laser welding of a CoCrFeMnNi high entropy alloy to 316 stainless steel. *Scr. Mater.* **2022**, *206*, 114219. [[CrossRef](#)]
20. Shao, H.B.; Huang, Y.C.; Liu, Y.; Ren, X.W.; Xiao, Z.B. Structural stabilities and thermal properties of η′–Mg₂Zn_{5–x}Al_{2+x} and η–MgZn₂ phase in Al–Zn–Mg alloy: First-principles calculation and quasi-harmonic Debye approximation. *J. Mater. Res. Technol.* **2021**, *10*, 840–852.